Skyrme-QRPA calculations for low-lying excitation modes in deformed neutron-rich nuclei

Kenichi Yoshida

Nishina Center for Accelerator-Based Science, RIKEN, Wako, Saitama 351-0198, Japan

Abstract. Low-frequency modes of excitation in deformed neutron-rich nuclei are studied by means of the quasiparticle random-phase approximation on the Skyrme-Hartree-Fock-Bogoliubov mean field. We investigate the microscopic structure of the soft $K^\pi = 0^+$ modes systematically in neutron-rich Magnesium isotopes with $N = 22, 24, 26$ and 28 close to the drip line, and it is found that the strong collectivity in ^{34}Mg and ^{40}Mg is acquired due to the coherent coupling between the β vibration and the pairing vibration of neutrons. Microscopic structure of the $K^\pi = 2^+$ modes changes gradually associated with the location of the Fermi level of neutrons, and it is found that the proton particle-hole excitation generating the $\gamma-$vibrational mode in ^{24}Mg continues to play a key role in the near-drip-line nucleus ^{40}Mg. The low-frequency octupole excitations are also investigated and the microscopic mechanism for the enhancement of transition strengths is discussed.

PACS. 21.60.Jz Nuclear Density Functional Theory and extensions – 21.10.Re Collective levels – 21.60.Ev Collective models – 27.30.+t – 27.40.+z

1 Introduction

Collective motion in unstable nuclei has raised a considerable interest both experimentally and theoretically. This is because low-frequency modes of excitation are quite sensitive to the shell structure near the Fermi level, and we can expect unique excitation modes to emerge associated with the new spatial structures such as neutron skins and the novel shell structures that generate new regions of deformation [1].

In order to investigate new kinds of excitation modes in exotic nuclei, the random-phase approximation (RPA) based on the self-consistent mean field has been employed by many groups. (See Refs. [2,3,4] for extensive lists of references concerning the self-consistent RPA and mean-field calculations.) They are however largely restricted to spherical systems, and the low-frequency excitation modes in deformed neutron-rich nuclei remain mostly unexplored.

Recently, low-lying RPA modes in deformed neutron-rich nuclei have been investigated by several groups [5,6,7, 8,9,10,11,12,13]. These calculations, however, do not take into account the pairing correlations, or rely on the BCS approximation for pairing (except for Ref. [13]), which is inappropriate for describing the pairing correlations in drip line nuclei due to the unphysical nucleon gas problem [14]. Quite recently, we have developed a new framework of the self-consistent deformed quasiparticle-RPA (QRPA) based on the Skyrme-Hartree-Fock-Bogoliubov (HFB) mean field [15].

Presently, small excitation energies of the first 2^+ state and striking enhancements of $B(E2; 0_1^+ \to 2_1^+)$ in ^{32}Mg [16, 17] and ^{34}Mg [18,19,20] are under lively discussions in connection with the onset of quadrupole deformation, the breaking of $N = 20$ spherical magic number, the pairing correlation and the continuum coupling effects [21,22,23, 24,25]. In order to get clear understanding of the nature of quadrupole deformation and pairing correlations, it is strongly desired to explore, both experimentally and theoretically, excitation spectra of these nuclei toward a drip line [26,27,28,29,30,31,32].

In this paper, we apply the new calculation scheme to the low-frequency excitation modes in neutron-rich Magnesium isotopes close to the drip line, and investigate the microscopic mechanism of the excitation modes uniquely appearing in deformed neutron-rich nuclei.

The paper is organized as follows: In Sec. 2, the deformed Skyrme-HFB + QRPA method is recapitulated. In Sec. 3, results of numerical analysis of the low-lying excitation modes in deformed neutron-rich Magnesium isotopes are presented. Finally, summary is given in Sec. 4.

2 Method

2.1 Skyrme-HFB in cylindrical coordinates

In order to describe simultaneously the nuclear deformation and the pairing correlations including the unbound

quasiparticle states, we solve the HFB equations [14,33]

$$
\begin{pmatrix} h^q(\boldsymbol{r},\sigma) - \lambda^q & \tilde{h}^q(\boldsymbol{r},\sigma) \\ \tilde{h}^q(\boldsymbol{r},\sigma) & -(h^q(\boldsymbol{r},\sigma) - \lambda^q) \end{pmatrix} \begin{pmatrix} \varphi_{1,\alpha}^q(\boldsymbol{r},\sigma) \\ \varphi_{2,\alpha}^q(\boldsymbol{r},\sigma) \end{pmatrix}
$$
$$
= E_\alpha \begin{pmatrix} \varphi_{1,\alpha}^q(\boldsymbol{r},\sigma) \\ \varphi_{2,\alpha}^q(\boldsymbol{r},\sigma) \end{pmatrix} \quad (1)
$$

in coordinate space using cylindrical coordinates $\boldsymbol{r} = (\rho, z, \phi)$. We assume axial and reflection symmetries. Here, $q = \nu$ (neutron) or π (proton). For the mean-field Hamiltonian h, we employ the SkM* interaction [34]. Details for expressing the densities and currents in the cylindrical coordinate representation can be found in Ref. [35]. The pairing field is treated by using the density-dependent contact interaction [36],

$$
v_{pair}(\boldsymbol{r},\boldsymbol{r}') = \frac{1-P_\sigma}{2}\left[t_0' + \frac{t_3'}{6}\varrho_0^\gamma(\boldsymbol{r})\right]\delta(\boldsymbol{r}-\boldsymbol{r}'). \quad (2)
$$

where $\varrho_0(\boldsymbol{r})$ denotes the isoscalar density of the ground state and P_σ the spin exchange operator. Assuming time-reversal symmetry and reflection symmetry with respect to the $x-y$ plane, we have to solve for positive Ω and positive z only, Ω being the $z-$component of the angular momentum j. We use the lattice mesh size $\Delta\rho = \Delta z = 0.6$ fm and a box boundary condition at $\rho_{\max} = 9.9$ fm, $z_{\max} = 12$ fm. The differential operators are represented by use of the 11-point formula of Finite Difference Method. Because the parity and Ω are good quantum numbers in the present calculation scheme, we have only to diagonalize the HFB Hamiltonian (1) for each Ω^π sector. The quasiparticle energy is cut off at $E_{\mathrm{qp,cut}} = 60$ MeV and the quasiparticle states up to $\Omega^\pi = 15/2^\pm$ are included.

The pairing strength parameter t_0' is determined so as to reproduce the experimental pairing gap of ^{34}Mg ($\Delta_{\exp} = 1.7$ MeV) obtained by the three-point formula [37]. The strength $t_0' = -295$MeV·fm^3 for the mixed-type interaction ($t_3' = -18.75 t_0'$) [38] with $\gamma = 1$ leads to the pairing gap $\langle \Delta_\nu \rangle = 1.71$ MeV in ^{34}Mg.

2.2 Quasiparticle-basis QRPA

Using the quasiparticle basis obtained as the self-consistent solution of the HFB equations (1), we solve the QRPA equation in the matrix formulation [39]

$$
\sum_{\gamma\delta} \begin{pmatrix} A_{\alpha\beta\gamma\delta} & B_{\alpha\beta\gamma\delta} \\ B_{\alpha\beta\gamma\delta} & A_{\alpha\beta\gamma\delta} \end{pmatrix} \begin{pmatrix} f_{\gamma\delta}^n \\ g_{\gamma\delta}^n \end{pmatrix} = \hbar\omega_n \begin{pmatrix} 1 & 0 \\ 0 & -1 \end{pmatrix} \begin{pmatrix} f_{\alpha\beta}^n \\ g_{\alpha\beta}^n \end{pmatrix}. \quad (3)
$$

The residual interaction in the particle-hole (p-h) channel appearing in the QRPA matrices A and B is derived from the Skyrme density functional. We neglect the spin-orbit interaction term $C_t^{\nabla J}$ as well as the Coulomb interaction to reduce the computing time. We also drop the so-called "J^2" term C_t^T both in the HFB and QRPA calculations. The residual interaction in the particle-particle (p-p) channel is derived from the pairing functional constructed with the density-dependent contact interaction (2).

Because the full self-consistency between the static mean-field calculation and the dynamical calculation is broken by the above neglected terms, we renormalize the residual interaction in the p-h channel by an overall factor f_{ph} to get the spurious $K^\pi = 0^-$ and 1^- modes (representing the center-of-mass motion), and $K^\pi = 1^+$ mode (representing the rotational motion in deformed nuclei) at zero energy ($v_{\mathrm{ph}} \to f_{\mathrm{ph}} \cdot v_{\mathrm{ph}}$). We cut the two-quasiparticle (2qp) space at $E_\alpha + E_\beta \leq 60$ MeV due to the excessively demanding computer memory size and computing time for the model space consistent with that adopted in the HFB calculation; $2E_{\mathrm{qp,cut}} = 120$ MeV. Accordingly, we need another factor f_{pp} for the p-p channel. We determine this factor such that the spurious $K^\pi = 0^+$ mode associated with the particle number fluctuation (representing the pairing rotational mode) appears at zero energy ($v_{\mathrm{pp}} \to f_{\mathrm{pp}} \cdot v_{\mathrm{pp}}$). (See Ref. [15] for details of determination of the normalization factors.)

In the present calculation, the dimension of the QRPA matrix (3) for the quadrupole $K^\pi = 0^+$ excitation in ^{40}Mg is about 16 400, and the memory size is 24.2 GB. The normalization factors are $f_{\mathrm{ph}} = 1.106$, and $f_{\mathrm{pp}} = 1.219$.

In terms of the nucleon annihilation and creation operators in the coordinate representation, $\hat{\psi}(\boldsymbol{r}\sigma)$ and $\hat{\psi}^\dagger(\boldsymbol{r}\sigma)$, the quadrupole operator is represented as

$$
\hat{Q}_{2K} = \sum_\sigma \int d\boldsymbol{r}\, r^2 Y_{2K}(\hat{r})\hat{\psi}^\dagger(\boldsymbol{r}\sigma)\hat{\psi}(\boldsymbol{r}\sigma). \quad (4)
$$

The intrinsic matrix elements $\langle n|\hat{Q}_{2K}|0\rangle$ of the quadrupole operator between the excited state $|n\rangle$ and the ground state $|0\rangle$ are given by

$$
\langle n|\hat{Q}_{2K}|0\rangle = \sum_{\alpha\beta} Q_{2K,\alpha\beta}^{\mathrm{(uv)}}(f_{\alpha\beta}^n + g_{\alpha\beta}^n) = \sum_{\alpha\beta} M_{2K,\alpha\beta}^{\mathrm{(uv)}}. \quad (5)
$$

The explicit expression of $Q_{2K,\alpha\beta}^{\mathrm{(uv)}}$ is given in Ref. [32]. The neutron (proton) matrix element M_ν (M_π) is defined

$$
M_\nu = \sum_{\alpha\beta\in\nu} M_{2K,\alpha\beta}^{\mathrm{(uv)}}, \qquad M_\pi = \sum_{\alpha\beta\in\pi} M_{2K,\alpha\beta}^{\mathrm{(uv)}}. \quad (6)
$$

2.3 Elimination of the spurious center-of-mass modes

It is known that the self-consistent RPA, if the same effective interaction or the same energy density functional is used exactly both for the ground state and for the excited state, restores translational invariance [40]. Because the present calculation scheme is not fully self-consistent, the calculated states $|n\rangle$ for $K^\pi = 0^-$ and 1^- excitations may contain the spurious component of the center-of-mass motion. In order to separate the intrinsic excitations from the spurious excitation, the "physical" states $|\tilde{n}\rangle$ are assumed

$$
\hat{X}_{\tilde{n}} = \hat{X}_n - \chi_P^n \hat{P} - \chi_R^n \hat{R}, \quad (7)
$$

where $\hat{X}_n$ is an annihilation operator of the calculated RPA mode, $\hat{R}$ and $\hat{P}$ are the coordinate and momentum

operators of the whole nucleus ($[\hat{R}, \hat{P}] = i\hbar$). The coefficients χ are considered to be small because the spurious component is expected to reasonably decouple from the physical solutions. The physical states satisfy the following conditions.

1. The vacuum condition:

$$\hat{X}_{\tilde{n}}|0\rangle = 0 \qquad (8)$$

2. The decoupling condition:

$$\langle 0|[\hat{X}_{\tilde{n}}, \hat{P}]|0\rangle = 0, \langle 0|[\hat{X}_{\tilde{n}}, \hat{R}]|0\rangle = 0 \qquad (9)$$

These conditions determine the coefficients χ_P^n, χ_R^n;

$$\chi_P^n = i\langle 0|[\hat{X}_n, \hat{R}]|0\rangle/\hbar, \chi_R^n = -i\langle 0|[\hat{X}_n, \hat{P}]|0\rangle/\hbar. \qquad (10)$$

The orthonormality of the physical states $|\tilde{n}\rangle$ satisfies in first order of the correction coefficient χ;

$$\begin{aligned}
\langle \tilde{n}|\tilde{m}\rangle &= \langle 0|[\hat{X}_{\tilde{n}}, \hat{X}_{\tilde{m}}^\dagger]|0\rangle \\
&= \langle 0|[\hat{X}_n, \hat{X}_m^\dagger]|0\rangle - i\hbar(\chi_P^n\chi_R^{m*} - \chi_R^n\chi_P^{m*}) \\
&\simeq \delta_{n,m}.
\end{aligned} \qquad (11)$$

In the actual calculations, the correction coefficient χ^2 is at most of order 10^{-5}. Separation of the spurious modes is also proposed in Ref. [41] in a similar way to the transition density.

The explicit expressions for calculating the matrix elements of the octupole transition operator are given in Appendix.

3 Results and discussion

3.1 Ground state properties

In Table 1, the ground state properties are summarized. The neutron-rich Magnesium isotopes under investigation

Table 1. Ground state properties of ^{34,36,38,40}Mg obtained by the deformed HFB calculation with the SkM* interaction and the mixed-type pairing interaction. Chemical potentials, deformation parameters, average pairing gaps, root-mean-square radii for neutrons and protons are listed. The average pairing gaps of protons are zero in these isotopes. The average pairing gap is defined $\langle\Delta\rangle_q = -\int dr\tilde{\varrho}/\int dr\tilde{\varrho}$.

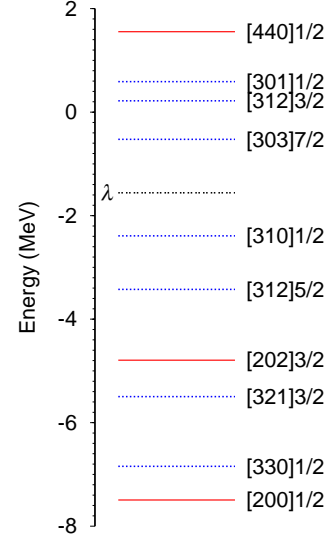|	^{34}Mg	^{36}Mg	^{38}Mg	^{40}Mg
λ_ν (MeV)	-4.16	-3.24	-2.41	-1.56
λ_π (MeV)	-19.8	-21.0	-23.7	-24.4
β_2^ν	0.35	0.31	0.29	0.28
β_2^π	0.41	0.39	0.38	0.36
$\langle\Delta\rangle_\nu$ (MeV)	1.71	1.71	1.64	1.49
$\sqrt{\langle r^2\rangle_\nu}$ (fm)	3.51	3.59	3.67	3.76
$\sqrt{\langle r^2\rangle_\pi}$ (fm)	3.16	3.18	3.20	3.22

Fig. 1. Neutron single-particle levels in ^{40}Mg labeled with the asymptotic quantum numbers $[Nn_3\Lambda]\Omega$. The solid and dotted lines stand for the positive and negative parities. The chemical potential λ is indicated by the two-dotted line.

are prolately deformed. This is consistent with the results calculated using the Skyrme SIII interaction except for ^{34}Mg [28]. The Gogny-HFB calculation suggested that ^{34}Mg is prolately deformed but soft against β deformation, and the shape coexistence in ^{38,40}Mg [31]. We can see that the neutron skin develops as approaching the drip line; the difference in neutron and proton radii $\sqrt{\langle r^2\rangle_\nu} - \sqrt{\langle r^2\rangle_\pi} = 0.35$ fm in ^{34}Mg changes to 0.54 fm in ^{40}Mg.

In Fig. 1, we show the neutron single-particle levels in ^{40}Mg. The single-particle states are obtained by rediagonalizing the self-consistent single-particle Hamiltonian $h[\varrho, \tilde{\varrho}]$ of Eq. (1). According to the present calculation employing the SkM* Skyrme density functional and the mixed-type pairing density functional, ^{40}Mg is located close to the neutron drip line.

3.2 Quadrupole vibrations

Figure 2 shows the intrinsic isoscalar quadrupole transition strengths in neutron-rich Mg isotopes for $K^\pi = 0^+$ and 2^+ excitations. For the $K^\pi = 0^+$ excitation, we can see a prominent peak possessing about 30 and 23 in Weisskopf unit below the threshold energy in ^{34}Mg and ^{40}Mg. If we assume the strong deformation limit [42], these intrinsic isoscalar transition strengths correspond to the transition strengths from the ground 0_1^+ state to the 2_β^+ state built on the excited $K^\pi = 0^+$ state, and those from the excited $K^\pi = 0^+$ state to the 2_1^+ state built on the ground 0_1^+ state in the laboratory frame.

On the other hand, we obtain the collective state in all of the isotopes for the $K^\pi = 2^+$ excitation.

In Table 2, we summarize the ratio of the matrix elements for neutrons and protons normalized by that of the neutron and proton numbers, $(M_\nu/M_\pi)/(N/Z)$, for the
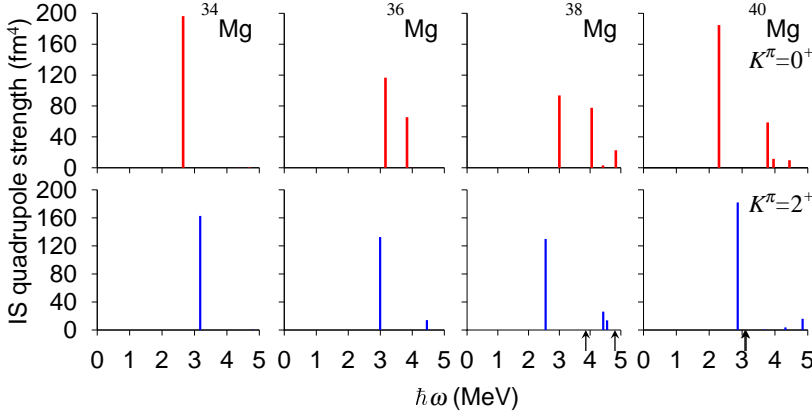
Fig. 2. Intrinsic isoscalar quadrupole transition strengths in ^{34,36,38,40}Mg for $K^\pi = 0^+$ (upper panel) and 2^+ (lower panel) excitations. The arrows indicate the neutron emission threshold energies. The one-neutron emission threshold energy is $E_{\mathrm{th},1n} = 3.86$ MeV and 3.09 MeV, and the two-neutron emission threshold energy is $E_{\mathrm{th},2n} = 4.81$ MeV and 3.12 MeV in ^{38}Mg and ^{40}Mg, respectively.

Table 2. Ratios of the neutron and proton matrix elements M_ν/M_π divided by N/Z for the lowest excited states in Mg isotopes for the quadrupole $K^\pi = 0^+$ and 2^+ excitations.

	^{34}Mg	^{36}Mg	^{38}Mg	^{40}Mg
$K^\pi = 0^+$	1.57	1.58	1.82	1.91
$K^\pi = 2^+$	1.41	1.41	1.55	1.79

lowest excitation modes. As approaching the neutron drip line, the contribution of the neutron excitation becomes large. This is one of the unique features of the excitation modes in drip-line nuclei and it is understood as follows: In drip-line nuclei, the neutron 2qp excitations dominantly take place outside of the nuclear surface. Therefore, the transition strengths of the 2qp excitation of neutrons become large. The proton p-h excitations, however, concentrate in the surface region. Consequently, coupling of the excitations between neutrons and protons becomes smaller, and the transition strengths of neutrons (M_ν^2) and protons (M_π^2) become extremely asymmetric. In Sec. 3.2.1, we discuss in detail the microscopic structure of the low-frequency $K^\pi = 0^+$ modes, and show the spatial structure of the excitations of neutrons and protons.

3.2.1 Soft $K^\pi = 0^+$ modes

In Fig. 3, we show the low-lying excitation spectra for the $K^\pi = 0^+$ states. Here excitation energies are evaluated by [43]

$$E(I, K) = \hbar\omega_{\mathrm{RPA}} + \frac{\hbar^2}{2\mathcal{J}_{\mathrm{TV}}}(I(I+1) - K^2), \qquad (12)$$

in terms of the vibrational frequencies ω_{RPA} and the Thouless-Valatin moment of inertia $\mathcal{J}_{\mathrm{TV}}$ calculated microscopically by the QRPA as described in Ref. [44]. As we can see in this figure, appearance of the soft $K^\pi = 0^+$ modes is quite sensitive to the neutron number.

In Ref. [44], we have discussed the generic feature of the low-lying $K^\pi = 0^+$ modes in deformed neutron-rich nuclei: In a deformed system where the up-sloping oblate-type and the down-sloping prolate-type orbitals exist near
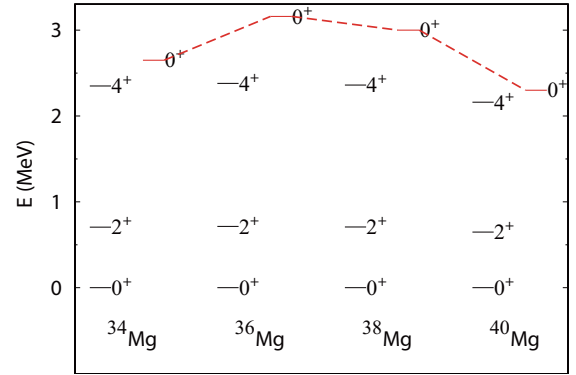

Fig. 3. Low-excitation energy spectra of ^{34,36,38,40}Mg.

the Fermi level, one obtains a low-lying mode possessing enhanced strengths both for the quadrupole p-h transition and for the quadrupole p-p (pair) transition induced by the pairing fluctuations. The up-sloping and down-sloping orbitals have quadrupole moments with opposite signs.

Generation mechanism of the soft $K^\pi = 0^+$ mode in deformed neutron-rich nuclei is understood essentially by the schematic two-level model in Ref. [42]. They consider the case where only two $\lambda\bar\lambda$ components are present in the wave functions both of the ground 0_1^+ and of the excited 0_2^+ states;

$$|K^\pi = 0_1^+\rangle = \frac{a}{\sqrt{a^2 + b^2}}|\lambda_1\bar\lambda_1\rangle + \frac{b}{\sqrt{a^2 + b^2}}|\lambda_2\bar\lambda_2\rangle \quad (13a)$$

$$|K^\pi = 0_2^+\rangle = -\frac{b}{\sqrt{a^2 + b^2}}|\lambda_1\bar\lambda_1\rangle + \frac{a}{\sqrt{a^2 + b^2}}|\lambda_2\bar\lambda_2\rangle. \quad (13b)$$

The transition matrix element for the quadrupole operator is then

$$\langle 0_1^+|\hat{Q}_{20}|0_2^+\rangle = \frac{2ab}{a^2 + b^2}[\langle\lambda_1|\hat{Q}_{20}|\lambda_1\rangle - \langle\lambda_2|\hat{Q}_{20}|\lambda_2\rangle] \quad (14)$$

and it is proportional to the difference in the quadrupole moments of the individual orbitals composing the 0^+ states. In the case that the quadrupole moments of the orbitals have opposite signs to each other, this matrix element becomes large. This situation is realized in the level crossing
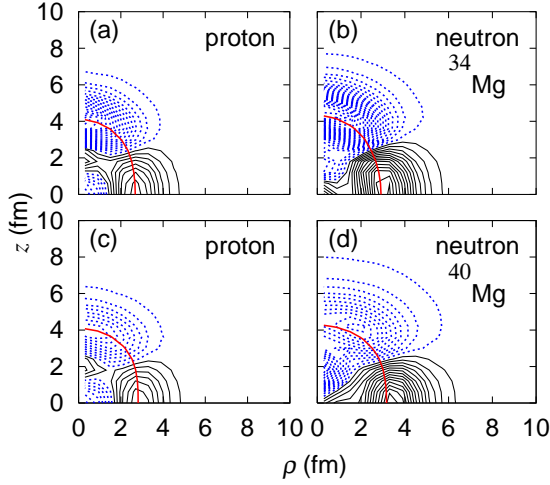
Fig. 4. Transition densities of protons (left) and neutrons (right) to the $K^\pi = 0^+$ states at 2.65 MeV in ^{34}Mg (upper) and at 2.30 MeV in ^{40}Mg (lower). Solid and dotted lines indicate positive and negative transition densities, and the contour lines are plotted at intervals of 3×10^{-4} fm^{-3}. The thick solid lines indicate the neutron and proton half densities of the ground state. They are 0.054 and 0.036 fm^{-3} for neutrons and protons, respectively in ^{34}Mg, and 0.055 and 0.032 fm^{-3} in ^{40}Mg.

Fig. 5. Transition strengths for the quadrupole-pair excitation in ^{40}Mg. The unperturbed 2qp transition strengths are shown in the lower panel.

region, where the up- and down-sloping orbitals exist. As the number of components increases in the QRPA calculations, the wave function becomes more complicated. It is discussed in Ref. [44].

In what follows, we investigate the microscopic structure of the low-lying $K^\pi = 0^+$ states, and discuss sensitivity to the location of the Fermi level of neutrons. Because the deformation properties of the Mg isotopes under investigation are not very different, Figure 1 is used for understanding the shell structure around the Fermi level.

In ^{34}Mg, we obtain the collective $K^\pi = 0^+$ mode at 2.65 MeV [15]. The transition strength is enhanced by 10.6 times as compared to the unperturbed transition strength. This mode is generated by many 2qp excitations, and among them the 2qp configurations of $(\nu[202]3/2)^2$ and $(\nu[321]3/2)^2$ have main contributions with weights of 0.44 and 0.34, respectively. The chemical potential is located between these two levels. They are a up-sloping and a down-sloping orbitals, respectively.

In ^{36}Mg, we obtain two weak-collective states. The second $K^\pi = 0^+$ state at 3.84 MeV is mainly generated by the 2qp excitations of $(\nu[321]3/2)^2$ and $(\nu[312]5/2)^2$ with weights of 0.48 and 0.35. The lowest $K^\pi = 0^+$ state at 3.17 MeV is analogous to the collective state in ^{34}Mg: This is mainly generated by the 2qp excitations of $(\nu[202]3/2)^2$ and $(\nu[310]1/2)^2$ with weights of 0.58 and 0.21, which are a up-sloping and a down-sloping levels, respectively.

We also obtain two weak-collective states in ^{38}Mg at 3.00 MeV and 4.05 MeV. The lower state has a similar structure to the lowest state in ^{36}Mg: This is mainly generated by the 2qp excitations of $(\nu[202]3/2)^2$ and $(\nu[310]1/2)^2$ with weights of 0.11 and 0.59. Furthermore, the 2qp excitation of $(\nu[312]5/2)^2$ has an appreciable contribution
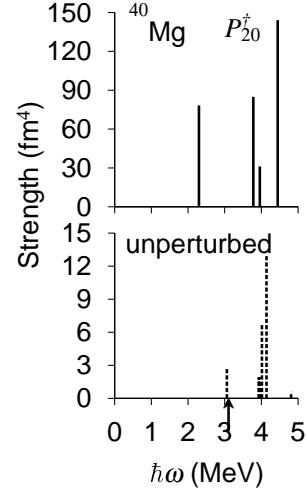
of 0.20. This excitation, however, acts destructively to the above excitations. Therefore the transition strength to the lowest state is not enhanced. The second $K^\pi = 0^+$ state is located just above the continuum threshold. This state is mainly generated by the excitations of $(\nu[303]7/2)^2$ and $(\nu[312]5/2)^2$ with weights of 0.38 and 0.34.

In ^{40}Mg, we can see a prominent peak at 2.30 MeV. This state is mainly generated by the excitations of $(\nu[310]1/2)^2$ and $(\nu[303]7/2)^2$ with weights of 0.50 and 0.29. The $\nu[303]7/2$ orbital is a up-sloping level stemming from the $1f_{7/2}$ orbital. Furthermore, many 2qp excitations of neutrons coherently participate in generating this soft $K^\pi = 0^+$ mode.

The transition densities to the soft $K^\pi = 0^+$ modes in ^{34}Mg and ^{40}Mg are shown in Fig. 4. Inside and around the nuclear surface denoted by the thick lines, neutrons and protons coherently oscillate along the symmetry axis (z−axis), indicating the β vibration. Furthermore, in neutrons only, we can see a spatially extended structure. The enhanced transition strength of neutrons is due to this spatial extension of the quasiparticle wave functions.

In order to see another interesting feature of the soft $K^\pi = 0^+$ mode in ^{40}Mg, we show in Fig. 5 the strength distributions of the quadrupole-pair transition defined by the operator

$$\hat{P}^\dagger_{20} = \int d\boldsymbol{r} r^2 Y_{20}(\hat{r}) \hat{\psi}^\dagger_\nu(\boldsymbol{r} \uparrow) \hat{\psi}^\dagger_\nu(\boldsymbol{r} \downarrow). \qquad (15)$$

The transition strength to the lowest state is enhanced about 28.4 times of the transition strength of the 2qp excitation $(\nu[310]1/2)^2$. The lowest $K^\pi = 0^+$ state in ^{40}Mg thus has a collective nature both in the p-h and p-p (pairing) channels.

3.2.2 $K^\pi = 2^+$ modes

Next, we investigate the microscopic structure of the $K^\pi = 2^+$ modes appearing at around 3 MeV.

In ^{34}Mg, two quasiparticle levels near the Fermi level, [202]3/2 and [321]3/2, play a dominant role in generating the $K^\pi = 2^+$ mode at 3.18 MeV: 2qp excitations of $\nu[202]3/2 \otimes \nu[220]1/2$ and $\nu[310]1/2 \otimes \nu[321]3/2$ have large contribution with weights of 0.51 and 0.14.

Because a [312]5/2 level is located close to the Fermi level in ^{36}Mg, the 2qp excitation of $\nu[310]1/2 \otimes \nu[312]5/2$ becomes a dominant component with a weight of 0.54. This component is not large in ^{34}Mg, which has 5% of the contribution. In ^{38}Mg, both of the [312]5/2 and [310]1/2 levels are close to the Fermi level. Therefore, the 2qp excitation of $\nu[310]1/2 \otimes \nu[312]5/2$ has larger contribution possessing a weight of 0.75. The 2qp excitation of $\nu[310]1/2 \otimes \nu[321]3/2$ still have an appreciable contribution with weights of 0.14 and 0.06 in ^{36}Mg and ^{38}Mg.

In ^{40}Mg, the 2qp excitation of $\nu[310]1/2 \otimes \nu[312]5/2$ has a large contribution with a weight of 0.24 similarly to the $K^\pi = 2^+$ states in ^{36}Mg and ^{38}Mg. Furthermore, because the [303]7/2 level is close to the Fermi level, the 2qp excitation of $\nu[312]3/2 \otimes \nu[303]7/2$ becomes a dominant component possessing 37% contribution.

In all of the $K^\pi = 2^+$ states in Mg isotopes under investigation, the proton p-h excitations also play an important role. Especially, the $\pi[211]3/2 \rightarrow \pi[211]1/2$ excitation has an appreciable contribution with weights of 0.21, 0.16, 0.09 and 0.09 in ^{34,36,38,40}Mg, respectively. It is noted that the γ-vibrational mode in ^{24}Mg is mainly generated by the neutron and proton p-h excitations of [211]3/2 → [211]1/2 [15].
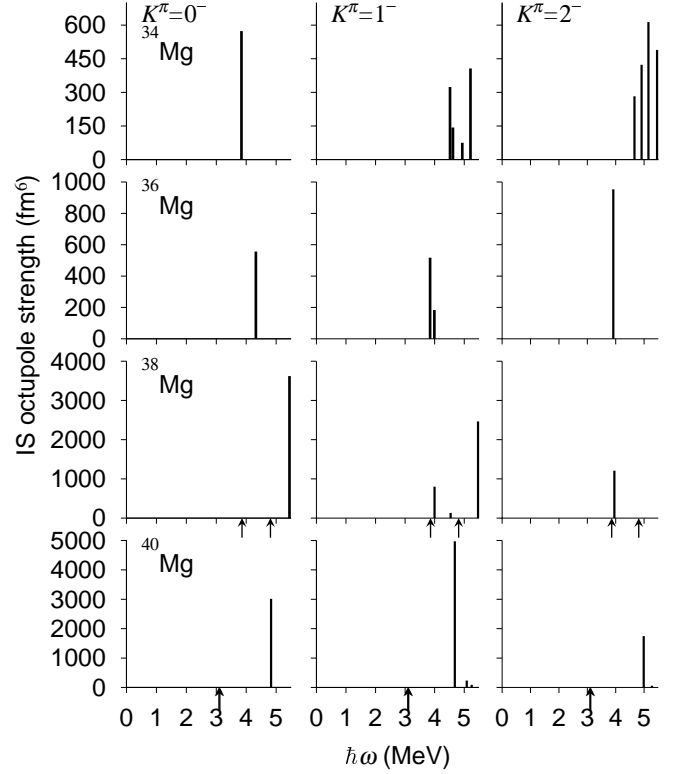

Fig. 6. Intrinsic isoscalar octupole transition strengths in ^{34,36,38,40}Mg for $K^\pi = 0^-$ (left panel), $K^\pi = 1^-$ (middle panel) and 2^- (right panel) excitations.

3.3 Octupole excitations

Figure 6 shows the intrinsic isoscalar octupole transition strengths. For the $K^\pi = 3^-$ excitations, there are no peaks representing strengths greater than 1 W.u. (1 W.u. is about 70–90 fm^6 in $^{34-40}$Mg) in the low-excitation energy region below 5 MeV.

Because the number of 2qp negative-parity excitations in this mass region is small as we can see the single-particle energy levels in Fig. 1, none of the excited states shown in Fig. 6 are collective. For instance, both of the lowest $K^\pi = 0^-$ states in ^{34}Mg and ^{36}Mg are generated by the $\nu[202]3/2 \otimes \nu[321]3/2$ excitation dominantly with a weight of 0.98. The unperturbed transition strength of this neutron 2qp excitation is about 20 fm^6. About 50% of the transition matrix element come from the coupling to the giant resonances around 10 MeV and 30 MeV.

In ^{38}Mg and ^{40}Mg, the lowest $K^\pi = 0^-$ state is generated by the $\nu[440]1/2 \otimes \nu[310]1/2$ excitation with weights of 0.72 and 0.88, respectively. In ^{38}Mg, the $\nu[202]3/2 \otimes \nu[321]3/2$ excitation still has a small contribution of 0.08. The transition strengths for the $K^\pi = 0^-$ excitation in ^{38}Mg and ^{40}Mg are about 5 times larger than in ^{34,36}Mg. This is because the unperturbed transition strengths of the neutron 2qp excitations below 10 MeV become extremely large due to the spatial extension of the quasiparticle wave functions around the Fermi level; the transition strength of the $\nu[440]1/2 \otimes \nu[310]1/2$ excitation is 313 fm^6 and 720 fm^6 in ^{38,40}Mg. Since the $\nu[310]1/2$ orbital is a

particle-like level in ^{38}Mg, the p-h transition strength is smaller than in ^{40}Mg. About 80% of the transition matrix element come from the neutron 2qp excitations below 10 MeV, and coupling to the giant resonance is small. In drip-line nuclei, the proton contribution is also small as in the case for the quadrupole excitations. In ^{40}Mg, the proton transition strength $B(E3; 0^+_{\rm gs} \rightarrow 3^-_{K^\pi=0^-})$ has only 5.0 e^2fm^6 whereas it has 33 e^2fm^6 in ^{34}Mg.

4 Summary

We have investigated the microscopic structure of the low-lying excitation modes systematically in neutron-rich Magnesium isotopes close to the drip line by means of the deformed Skyrme-QRPA method.

In the spherical neutron-rich nuclei, the effect of the dynamical pairing has been investigated in detail in Refs. [45, 46,47]. In Ref. [44], we showed the importance of the dynamical pairing in neutron-rich deformed systems. In a deformed system where the up- and down-sloping orbitals exist near the Fermi level, one obtains the low-lying mode possessing extremely enhanced strengths both for the quadrupole p-h transition and for the quadrupole p-p (pair) transition induced by the pairing fluctuation.

In this article, we demonstrated the importance of the dynamical pairing in deformed drip-line system. Not only

in ^{34}Mg but in ^{40}Mg, the soft $K^\pi = 0^+$ modes are generated by the neutron 2qp excitations of the up-sloping and down-sloping orbitals. And we found that the transition strength to the soft $K^\pi = 0^+$ modes is much enhanced not only for the quadrupole p-h excitation but also for the quadrupole p-p excitation.

We obtained the collective $K^\pi = 2^+$ excitations in all of the isotopes under investigation. As the neutron number increases, the contribution of neutron 2qp excitations to the $K^\pi = 2^+$ mode changes gradually according to the location of the Fermi level of neutrons. Furthermore, we found that the proton p-h excitation of $[211]3/2 \to [211]1/2$ creating the $\gamma-$vibrational mode in ^{24}Mg keeps playing an important role in generating the collective $K^\pi = 2^+$ modes even in the near-drip-line nuclei.

For the octupole excitations, we could not find any collective modes in the low-energy region. Despite the weak collectivity, the transition strengths are enhanced due to the microscopic mechanism: In ^{34}Mg and ^{36}Mg, coupling to the giant resonances at $1\hbar\omega_0$ and $3\hbar\omega_0$ gives rise to the enhancement of the transition strengths. In ^{38}Mg and ^{40}Mg close to the drip line, because the quasiparticle wave functions near the Fermi level have the spatially extended structure, the transition strengths of the neutron 2qp excitations become extremely large. However, the proton contribution becomes small in near-drip-line nuclei because the spatial overlap between the proton p-h excitations and neutron 2qp excitations is small.

Appendix

The transition strengths between the RPA ground $|0\rangle$ and the corrected "physical" state $|\tilde{n}\rangle$ for the operator $\hat{O}$ are calculated as

$$|\langle\tilde{n}|\hat{O}|0\rangle|^2 = |\langle 0|[X_{\tilde{n}}, \hat{O}]|0\rangle|^2. \qquad (A\text{-}1)$$

The transition matrix elements for the isoscalar octupole operator

$$\hat{O}_{3K} = \sum_\sigma \int d\boldsymbol{r} r^3 Y_{3K}(\hat{r})\hat{\psi}^\dagger(\boldsymbol{r}\sigma)\hat{\psi}(\boldsymbol{r}\sigma) \qquad (A\text{-}2)$$

are given as

$$\langle 0|[X_{\tilde{n}}, \hat{O}_{30}]|0\rangle$$
$$= \langle 0|[X_n, \hat{O}_{30}]|0\rangle$$
$$+ 2\pi i\hbar\chi^n_{P_z}\sqrt{\frac{7}{16\pi}}\int \rho d\rho dz\varrho_0(\rho, z)(6z^2 - 3\rho^2) \qquad (A\text{-}3)$$

for the $K^\pi = 0^-$ states and

$$\langle 0|[X_{\tilde{n}}, \hat{O}_{31}]|0\rangle$$
$$= \langle 0|[X_n, \hat{O}_{31}]|0\rangle$$
$$- 2\pi i\hbar\chi^n_{P_\rho}\sqrt{\frac{21}{64\pi}}\int \rho d\rho dz\varrho_0(\rho, z)(4z^2 - 3\rho^2) \qquad (A\text{-}4)$$

for the $K^\pi = 1^-$ states. Here

$$\chi^n_{P_z} = \frac{i}{\hbar}\frac{1}{A}\sum_{i=1}^A \langle 0|[X_n, \hat{z}_i]|0\rangle, \qquad (A\text{-}5)$$

$$\chi^n_{P_\rho} = \frac{i}{\hbar}\frac{1}{A}\sum_{i=1}^A \langle 0|[X_n, \hat{\rho}_i e^{i\phi}]|0\rangle. \qquad (A\text{-}6)$$

References

1. M. V. Stoitsov, J. Dobaczewski, W. Nazarewicz, S. Pittel, and D. J. Dean, Phys. Rev. C **68**, 054312 (2003).
2. M. Bender, P.-H. Heenen and P.-G. Reinhard, Rev. Mod. Phys. **75**, 121 (2003).
3. D. Vretenar, A. V. Afanasjev, G. A. Lalazissis and P. Ring, Phys. Rep. **409**, 101 (2005).
4. N. Paar, D. Vretenar, E. Khan and G. Colò, Rep. Prog. Phys. **70**, 691 (2007).
5. K. Yoshida, M. Yamagami and K. Matsuyanagi, Prog. Theor. Phys. **113**, 1251 (2005).
6. T. Nakatsukasa and K. Yabana, Phys. Rev. C **71**, 024301 (2005).
7. T. Inakura, H. Imagawa, Y. Hashimoto, S. Mizutori, M. Yamagami and K. Matsuyanagi, Nucl. Phys. **A768**, 61 (2006).
8. P. Sarriguren, E. Moya de Guerra, A. Escuderos and A. C. Carrizo, Nucl. Phys. **A635**, 55 (1998).
9. O. Moreno, R. Álvarez-Rodríguez, P. Sarriguren, E. Moya de Guerra, J. M. Udías and J. R. Vignote, Phys. Rev. C **74**, 054308 (2006).
10. P. Urkedal, X. Z. Zhang and I. Hamamoto, Phys. Rev. C **64**, 054304 (2001).
11. K. Hagino, N. Van Giai and H. Sagawa, Nucl. Phys. **A731**, 264 (2004).
12. D. P. Arteaga and P. Ring, Prog. Part. Nucl. Phys. **59**, 314 (2007).
13. S. Péru and H. Goutte, Phys. Rev. C **77**, 044313 (2008).
14. J. Dobaczewski, H. Flocard and J. Treiner, Nucl. Phys. **A422**, 103 (1984).
15. K. Yoshida and N. Van Giai, Phys. Rev. C **78**, 064316 (2008).
16. D. Guillemaud-Müller *et al.*, Nucl. Phys. **A426**, 37 (1984).
17. T. Motobayashi *et al.*, Phys. Lett. **B346**, 9 (1995).
18. K. Yoneda *et al.*, Phys. Lett. **B499**, 223 (2001).
19. J. A. Church *et al.*, Phys. Rev. C **72**, 054320 (2005).
20. Z. Elekes *et al.*, Phys. Rev. C **73**, 044314 (2006).
21. A. Poves and J. Retamosa, Phys. Lett. **B184**, 311 (1987).
22. E. K. Warburton, J. A. Becker, and B. A. Brown, Phys. Rev. C **41**, 1147 (1990).
23. N. Fukunishi, T. Otsuka, and T. Sebe, Phys. Lett. **B296**, 279 (1992).
24. Y. Utsuno, T. Otsuka, T. Mizusaki, and M. Honma, Phys. Rev. C **60**, 054315 (1999).

25. M. Yamagami and N. Van Giai, Phys. Rev. C **69**, 034301 (2004).
26. A. Gade *et al.*, Phys. Rev. Lett. **99**, 072502 (2007).
27. T. Baumann *et al.*, Nature **449**, 1022 (2007).
28. J. Terasaki, H. Flocard, P.-H. Heenen, and P. Bonche, Nucl. Phys. **A621**, 706 (1997).
29. E. Caurier, F. Nowacki, A. Poves, and J. Retamosa, Phys. Rev. C **58**, 2033 (1998).
30. P.-G. Reinhard, D. J. Dean, W. Nazarewicz, J. Dobaczewski, J. A. Maruhn, and M. R. Strayer, Phys. Rev. C **60**, 014316 (1999).
31. R. Rodoríguez-Guzmán, J. L. Egido, L. M. Robledo, Nucl. Phys. **A709**, 201 (2002).
32. K. Yoshida, M. Yamagami and K. Matsuyanagi, Nucl. Phys. **A779**, 99 (2006).
33. A. Bulgac, Preprint No. FT-194-1980, Institute of Atomic Physics, Bucharest, 1980. [arXiv:nucl-th/9907088]
34. J. Bartel, P. Quentin, M. Brack, C. Guet and H.-B. Håkansson, Nucl. Phys. **A386**, 79 (1982).
35. E. Terán, V. E. Oberacker and A. S. Umar, Phys. Rev. C **67**, 064314 (2003).
36. R. R. Chasman, Phys. Rev. C **14**, 1935 (1976).
37. W. Satuła, J. Dobaczewski and W. Nazarewicz, Phys. Rev. Lett. **81**, 3599 (1998).
38. K. Bennaceur and J. Dobaczewski, Comput. Phys. Commun. **168**, 96 (2005).
39. D. J. Rowe, *Nuclear Collective Motion* (Methuen and Co. Ltd., 1970).
40. P. Ring and P. Schuck, *The Nuclear Many-Body Problem*, (Springer, 1980).
41. T. Nakatsukasa, T. Inakura, and K. Yabana, Phys. Rev. C **76**, 024318 (2007).
42. A. Bohr, B. R. Motteleson, *Nuclear Structure*, vol. II (Benjamin, 1975; World Scientific 1998).
43. J. M. Eisenberg and W. Greiner, *Nuclear Models*, vol. I (North Holland, 1970).
44. K. Yoshida and M. Yamagami, Phys. Rev. C **77**, 044312 (2008).
45. M. Matsuo, Nucl. Phys. **A696**, 371 (2001).
46. M. Matsuo, K. Mizuyama, and Y. Serizawa, Phys. Rev. C **71**, 064326 (2005).
47. N. Paar, P. Ring, T. Nikšić, and D. Vretenar, Phys. Rev. C **67**, 034312 (2003).